



Publication Year	2020
Acceptance in OA	2021-01-20T13:14:28Z
Title	Detection Capability of Flux Ropes during the Solar Orbiter Mission
Authors	TELLONI, Daniele, D'AMICIS, RAFFAELLA, BRUNO, Roberto, Carbone, Francesco, PERRONE, DENISE, Zank, Gary P., Zhao, Lingling, Nakanotani, Masaru, Adhikari, Laxman
Publisher's version (DOI)	10.3847/2041-8213/abacc4
Handle	http://hdl.handle.net/20.500.12386/29873
Journal	THE ASTROPHYSICAL JOURNAL LETTERS
Volume	899

Detection Capability of Flux Ropes during the *Solar Orbiter* MissionDANIELE TELLONI,¹ RAFFAELLA D'AMICIS,² ROBERTO BRUNO,² FRANCESCO CARBONE,³ DENISE PERRONE,⁴
GARY P. ZANK,^{5,6} LINGLING ZHAO,⁵ MASARU NAKANOTANI,⁵ AND LAXMAN ADHIKARI⁵¹*National Institute for Astrophysics - Astrophysical Observatory of Torino*
*Via Osservatorio 20, 10025 Pino Torinese, Italy*²*National Institute for Astrophysics - Institute for Space Astrophysics and Planetology*
*Via del Fosso del Cavaliere 100, 00133 Roma, Italy*³*National Research Council - Institute of Atmospheric Pollution Research*
*c/o University of Calabria, 87036 Rende, Italy*⁴*Italian Space Agency**Via del Politecnico snc, 00133 Roma, Italy*⁵*University of Alabama, Center for Space Plasma and Aeronomic Research*
*Huntsville, AL 35805, USA*⁶*University of Alabama, Department of Space Science*
Huntsville, AL 35805, USA

(Received August 3, 2020; Revised August 3, 2020; Accepted August 3, 2020)

Submitted to ApJ

ABSTRACT

Flux ropes are interplanetary magnetic helical structures that are receiving increasing attention because of their likely role in magnetohydrodynamic (MHD) processes as well as their impact on space weather science. A very promising and powerful approach to address their investigation and characterization is based on wavelet spectrograms of the invariants of the ideal MHD equations. The accuracy of this method to infer flux rope properties depends on the proper evaluation of the direction of propagation of the flux rope itself, which is often difficult to assess. We present a numerical test of the reliability of this diagnostic technique, by simulating a synthetic flux rope of fixed size and propagation direction along the *Solar Orbiter* orbit, that is very elongated and inclined with respect to the orbital plane. We find that when the flux rope is crossed for less than 50% of its **width**, the procedure becomes unreliable. Quantitative information on how to properly recover the flux-rope intrinsic properties is provided.

Keywords: Magnetohydrodynamics (MHD) — Methods: data analysis — Space vehicles — Sun: coronal mass ejections (CMEs) — solar wind — Interplanetary medium

1. INTRODUCTION

Flux ropes are twisted magnetic structures with a force-free field configuration in which the current density $\mathbf{J} = \nabla \times \mathbf{B}/\mu_0$ (μ_0 is the magnetic permeability in vacuum) is parallel to the magnetic field \mathbf{B} , i.e. $\mathbf{J} = \alpha\mathbf{B}$ (where α is a constant parameter, Goldstein 1983; Lepping et al. 1990). Because of their helical magnetic configuration, flux ropes store and carry high levels of magnetic helicity (H_m), the ideal magnetohydrodynamical (MHD) invariant that quantifies the twist of magnetic field lines (Moffat 1978). This is defined as:

$$H_m = \int_{\Omega} \mathbf{A} \cdot \mathbf{B} \, d\Omega, \quad (1)$$

where \mathbf{A} is the vector potential ($\mathbf{B} = \nabla \times \mathbf{A}$) and the integral is computed over the closed volume Ω of the flux rope, at whose borders $\mathbf{n} \cdot \mathbf{B} = 0$, with \mathbf{n} the normal to the surface. It is worth noting that maximum helicity states, applying

when $\mathbf{B} \propto \mathbf{A}$, hold for force-free structures such as flux ropes: indeed, H_m is maximized when \mathbf{B} is (anti)parallel to \mathbf{A} and, in turn, to \mathbf{J} , typical of a force-free field.

Flux ropes, which are observed to permeate the solar wind from the inner to the distant heliosphere (Feng et al. 2007; Cartwright & Moldwin 2010; Telloni et al. 2012, 2013, 2016, 2019; Yu et al. 2014; Zheng & Hu 2018; Hu et al. 2018; Chen et al. 2019; Zhao et al. 2019a, 2020), have over last few years attracted great interest from the scientific community for many crucial reasons, including i) revealing the physical processes underlying their origin; ii) casting light on the dynamical evolution of incompressible MHD; iii) understanding turbulence in the corona and how it is transported throughout the heliosphere; iv) investigating associated particle acceleration, and finally v) improving the detection of solar Coronal Mass Ejections (CMEs) in the framework of space weather science.

The origin of flux ropes is indeed still extensively debated. Whether they are generated locally in the interplanetary plasma, via magnetic reconnection across the heliospheric current sheet and/or via plasma instabilities (e.g., Kelvin-Helmholtz instability, not yet observed in situ but theoretically predicted to occur, Mishin & Tomozov 2016), or are formed in the solar corona, being either the interplanetary counterparts of small solar eruptions (eventually too faint to be detectable in coronagraphic images, Feng et al. 2007) or the remnants of plasma blobs disconnected (via the linear tearing-mode instability) from equatorial streamers (Wang et al. 1998, although a one-to-one correlation of a coronal blob and a small-scale flux rope in the solar wind has not yet been observed), is still an open question. Thus, extensive investigation of flux ropes in the solar wind will advance our knowledge about the physical mechanisms underlying their generation and evolution.

Flux ropes may also arise from the decay of an ideal magnetofluid. Indeed, an incompressible MHD fluid may relax at large scales towards a maximum magnetic helicity state (Ting et al. 1986; Carbone & Veltri 1992), which, as discussed above, corresponds to a force-free field. During the relaxation process of magnetized fluids, the invariants of the ideal MHD equations, namely the magnetic helicity, the cross-helicity (which is a measure of the direction of propagation of the flux of Alfvénic fluctuations) and the total (magnetic plus kinetic) energy, play a crucial role (Woltjer 1958). By evaluating MHD invariants within a statistical sample of flux ropes identified in space plasma at 1 AU, Telloni et al. (2016) provided observational evidence that flux ropes naturally emerge from the inverse cascade undergone by the magnetic helicity (Frisch et al. 1975) towards ordered large-scale force-free magnetic structures, as usually observed in laboratory plasmas (Taylor 1974; Gray et al. 2013). Characterizing flux ropes in terms of the ideal MHD invariants will clarify the role played by ideal MHD selective decay in generating large-scale, force-free structures in space plasma.

The study of flux ropes is of paramount importance also in addressing fundamental questions regarding solar wind turbulence. Indeed, one of the most widely used models to describe turbulence and its transport from the photosphere to the solar corona and beyond, advanced by Zank et al. (2018), is based on the idea that turbulence consists of predominant quasi-2D magnetic flux rope-like structures and a minority slab (Alfvénic) component (Zank et al. 2017). The quasi-2D structures are formed in the lowest atmosphere by photospheric transverse flow motions, which lead the magnetic fields to become highly twisted (Parker 1988, 1994). As a consequence of the magnetic field winding, magnetic reconnection may occur at the newborn current sheets in the magnetic carpet, driving the formation and rapid dynamical evolution of quasi-2D helical plasmoids. Since a promising mechanism for heating the coronal plasma and accelerating the solar wind is the dissipation of high-frequency Alfvén waves, likely via ion-cyclotron resonance scattering, as indicated by numerous studies based on UVCS coronal observations (e.g., Cranmer et al. 1999), understanding how waves and turbulence are generated and transported from the photosphere to the outer layers of the solar atmosphere and the role played by magnetic flux rope-like structures in these processes is thus central to the coronal heating problem.

Dynamically interacting magnetic flux ropes are an emerging paradigm for the energization of charged particles throughout the heliosphere. Recent studies suggest that the observed unusual energetic particle flux enhancements at the leading edge of interplanetary CMEs, downstream of the shocks and near the heliospheric current sheet might be related to reconnection-based local acceleration in a dynamic multi-flux ropes environment (Zhao et al. 2018, 2019a,b; Adhikari et al. 2019). Charged particles can be energized through a first- or second-order Fermi process due to the contraction or merging of magnetic flux ropes. The stochastic transport theory developed by Zank et al. (2014, 2015) and later extended in Zhao et al. (2018) showed that reconnection processes associated with magnetic flux rope interaction can successfully explain the observed unusual energetic ion events in the solar wind.

Finally, space weather science will benefit from an in-depth investigation of flux ropes. Indeed, it has been recently proved that flux ropes universally represent the core magnetic structure of any CME (Vourlidas 2014). Hence, as first exploited by Telloni et al. (2019), the possibility of properly localizing CME events by identifying the magnetic

helicity content carried by the embedded flux ropes represents a novel opportunity for providing advance warning of Earth-directed CMEs likely to cause geomagnetic storms.

To address the topics outlined above, some crucial information is required. This comprises the flux rope duration (say its size), its characteristic scale, and the content of some MHD quantities, namely the magnetic helicity, cross-helicity and residual energy (which is a measure of the imbalance between kinetic and magnetic energies). These last two quantities are essential in distinguishing flux ropes (representing quasi-2D turbulence) from Alfvénic structures (characteristic of slab turbulence), which may be mistaken observationally as flux ropes because of their common helical magnetic field configuration (and, in turn, magnetic helicity signature). However, in the case of Alfvénic structures, the cross-helicity is high, indicating propagating fluctuations at the local Alfvén speed, while the residual energy is close zero because of energy equipartition, typical of Alfvén waves. By contrast, flux ropes are characterized by very low cross-helicity (as they are non-propagating structures advected by the solar wind) and by highly negative residual energy, as expected for magnetic fluctuation dominated structures. A diagnostic technique for localizing flux ropes in the solar wind plasma and characterizing them in terms of the MHD invariants was proposed by [Telloni et al. \(2012\)](#), and extensively used later by [Telloni et al. \(2013, 2016\)](#) in a statistical analysis of the MHD properties of flux ropes identified at 1 AU in *Wind* data. This approach was recently adopted by [Zhao et al. \(2020\)](#) to search for flux ropes in the *Parker Solar Probe* measurements during its first orbit around the Sun, thus providing novel information about the nature of these structures in the pristine solar wind. This method is specifically based on the construction of wavelet spectrograms of the magnetic helicity, cross-helicity, and residual energy. The decomposition of magnetic field and plasma parameters time series into time-frequency space allows for the determination of both the dominant scales of the magnetic field braiding and energy predominance as well as the corresponding magnetic helicity and residual energy modulation in time ([Torrence & Compo 1998](#)).

In spite of its undoubted potential, this technique suffers from a major limitation. Its ability to properly quantify the geometrical and MHD properties of the flux rope depends strictly on the inclination between the direction of propagation of the flux rope itself and the sampling direction of the spacecraft, i.e. on the part of the structure crossed by the probe. This means that for spacecraft (like *Wind*) orbiting around the Lagrangian point L1 at a fixed heliocentric distance of 1 AU and whose sampling direction always lies in the ecliptic plane, the greatest source of inaccuracy lies in the largely unknown direction of propagation of the structure. The uncertainty in the quantities inferred through this approach would increase significantly if the spacecraft had a trajectory that was not in the ecliptic and if its elevation above the equatorial plane varied considerably during its orbit around the Sun. It appears evident that in this case the reliability of this diagnostic method would depend also on the orbital parameters (distance from the Sun and heliographic latitude) of the spacecraft and not only on the propagation direction of the flux rope. During its mission, *Solar Orbiter* will experience multiple Venus gravitational assists that will push its orbit closer to the Sun and lift it out of the ecliptic. How do the different orbital parameters affect the measure of the size and scale of flux ropes? To what extent can this technique be satisfactorily used to search for these interplanetary structures at different heliocentric distances and heliographic latitudes in *Solar Orbiter* data? What is the uncertainty introduced in the analysis along the *Solar Orbiter* trajectory? If and how can intrinsic flux-rope quantities be properly recovered?

To attempt to answer the above question, a synthetic flux rope with fixed direction of propagation pointing towards Earth is modeled as it evolves over distance throughout the inner heliosphere. Encounters (if any) with the *Solar Orbiter* spacecraft during its orbit around the Sun are simulated to test the efficacy of the [Telloni et al. \(2012\)](#) technique and to investigate how the characterization of the flux rope properties depends on heliodistance and proximity to the equatorial plane of the probe. This will resolve how to address the problem of the generation and evolution of flux ropes, as well as of their contribution to overall turbulence in the solar wind. **As a matter of fact, since the theory of nearly incompressible MHD incorporates intrinsically quasi-2D flux rope-like structures ([Zank et al. 2017](#)), it is evident that the study of their MHD properties, using the diagnostic method developed by [Telloni et al. \(2012\)](#), is crucial in the context of turbulence generation and transport.** This is the aim of this paper, which is organized as follows: description of the synthetic flux rope and of *Solar Orbiter*'s orbit (§ 2), numerical test of the performance of the technique (§ 3), discussion of the results and concluding remarks (§ 4).

2. SYNTHETIC FLUX ROPE AND *SOLAR ORBITER*'S ORBIT

According to the constant- α force-free field model, a synthetic flux rope can be described as magnetic field lines wrapped around a cylindrically symmetric tube-like shape ([Russell & Elphic 1979](#)). Its schematic representation, along with the geometry of the spacecraft crossing, is shown in the cartoon of Fig. 1.

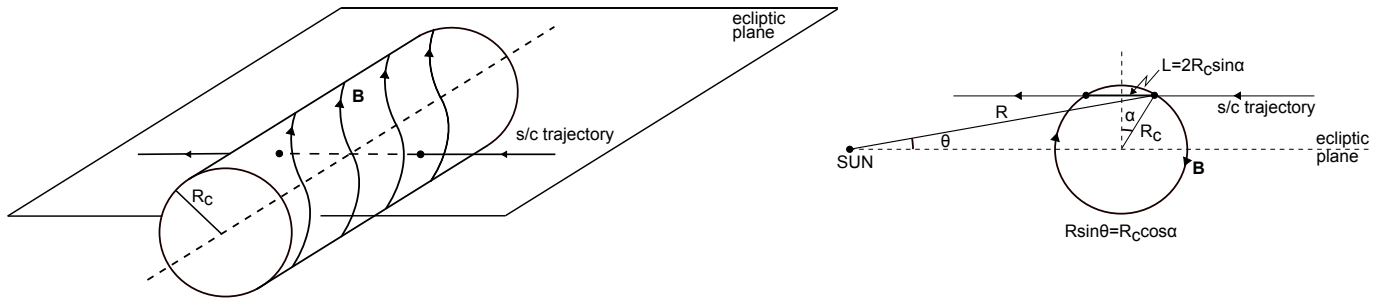


Figure 1. Cartoon of a flux rope with a helical magnetic field configuration, crossed by the spacecraft (*left*); the portion of the structure crossed by the probe, which has an elevation θ from the ecliptic plane and a distance R from the Sun, is $L = 2R_C \sin \alpha$, where R_C is the radius of the flux rope and α is defined by the relation $R \sin \theta = R_C \cos \alpha$ (*right*).

The flux rope is modeled as propagating in the ecliptic (namely, its direction of propagation lies in the equatorial plane). As illustrated in the cartoon in the right panel of Fig. 1, the probe crosses the structure for a **section** L that depends on its distance R from the Sun and its elevation θ in the orbital plane. From simple geometrical considerations, $L = 2R_C \sin \alpha$, where R_C is the size of the flux rope (say the radius of the tube-like bent magnetic field lines) and α is the angle such that $R \sin \theta = R_C \cos \alpha$. Hence, $L = 2R_C \sin(\arccos(R \sin \theta / R_C))$. Observations of the same flux rope at different solar distances during a radial alignment of two or more spacecraft are very rare. Hence, there is no consensus as whether or not these structures expand during their propagation in the solar wind. For instance, [Cartwright & Moldwin \(2010\)](#) found, on the basis of a statistical study of different flux ropes observed at different heights by different probes, that the mean size of these objects follows as $R^{0.43}$. On the other hand, more recently, [Janvier et al. \(2014\)](#) found no in-situ evidences for flux rope expansion. Therefore, to a first approximation, the synthetic flux rope is assumed not to expand and, in turn, R_C is held constant with heliocentric distance (**this allows the test of the reliability of the technique regardless of the flux rope dimension**); **specifically, in order to cover the full spectrum of all possible spacecraft crossings, R_C has been chosen such that at some point along *Solar Orbiter*'s orbit, the spacecraft's trajectory would be almost tangent to the flux rope. This means that $R_C = \max(R \sin \theta) = 0.29$ AU. As a matter of fact, if the tube-like flux rope had a size of 0.29 AU and lay in the ecliptic, it results that *Solar Orbiter* would always encounter it, spanning from crossing it for all the entire width (say the diameter) to barely touching it.** The constant value assumed for R_C implies that L is a function solely of $R \sin \theta$, i.e. $L = L(R \sin \theta)$.

During its mission, *Solar Orbiter* will approach the Sun as close as 0.28 AU and will be above the ecliptic plane by as much as 29° . Figure 2 displays where *Solar Orbiter* will be on April 8, 2023, when the spacecraft is at a distance of 0.29 AU from the Sun and is 5° below the ecliptic. The upper panels display its position and the previous year's trajectory, as projected on the XZ (on the left) and XY (or orbital, on the right) planes in the heliocentric ecliptic coordinate frame, also with respect to Earth and Venus (the discontinuity in *Solar Orbiter*'s orbit is due to the first Venus gravity assist maneuver experienced by the probe at the end of 2020). Bottom-left and -right panels of Fig. 2 show, respectively, the heliocentric distance and the elevation of the orbital plane of *Solar Orbiter* as a function of time for the whole mission.

Because of its inclined orbit, during its 22 close approaches to the Sun, *Solar Orbiter* will repeatedly go above and below the ecliptic plane, progressively increasing its elevation to it.

In Geocentric Solar Ecliptic (GSE) Cartesian coordinates (where the x -axis points towards the Sun, the z -axis is perpendicular to the ecliptic plane, and the y -axis completes the right-handed orthogonal set), flux ropes are generally observed in satellite data as half-rotations in the magnetic field direction around the x -axis (e.g., [Feng et al. 2007](#); [Telloni et al. 2012, 2013](#); [Zhao et al. 2020](#)). The transverse components of the magnetic field vector, B_y and B_z , of the synthetic flux rope have been thus modeled as sinusoidal functions $\pi/2$ out of phase (while B_x was assumed to have a constant profile). The flux rope can therefore be observed as a clockwise rotation of the magnetic field vector in the $y - z$ plane. Furthermore, as revealed by observations, the pitch of the magnetic field winding (say, the characteristic timescale of the synthetic flux rope) has been set to be twice the flux rope dimension, say of its diameter $2R_C$. **Since R_C has been assumed to be equal to 0.29 AU, it results that the magnetic helical pitch is 1.16 AU. Moving from space to time domain in the numerical test, R_C has been set to 64 data points (arbitrary**

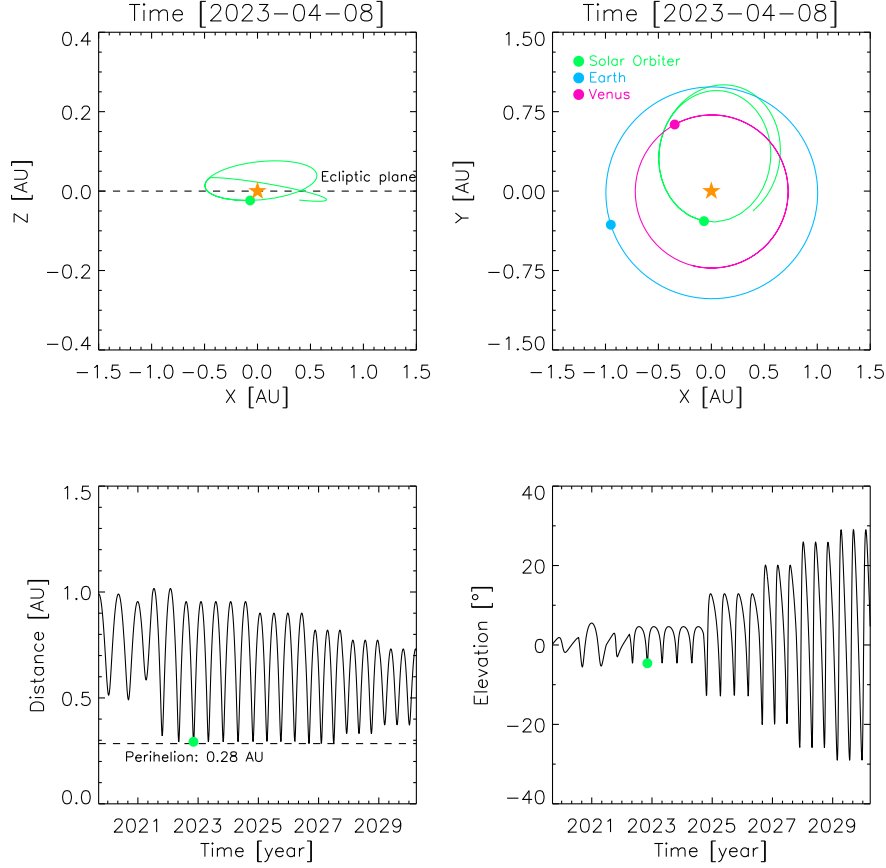


Figure 2. *Top panels:* trajectory of *Solar Orbiter* (green circle and line) from April 8, 2022 to April 8, 2023 around the Sun (yellow star), in XZ (*left*) and XY (*right*) planes of the heliocentric ecliptic coordinate frame; Venus’s and Earth’s orbits are also shown (with blue and pink colors, respectively) in the XY view. *Bottom panels:* heliocentric distance (*left*) and heliographic latitude (*right*) of the spacecraft as a function of time. Dots refer to April 8, 2023. An animated version of the figure is available online.

time units) and, in turn, the characteristic timescale to 256 data points. While these last two flux-rope parameters have been kept constant during *Solar Orbiter*’s orbit, radial dependences of $B_x \sim R^{-2}$, $B_y \sim R^{-1.2}$, and $B_z \sim R^{-1.4}$ have been assumed for the x -, y -, and z - magnetic field components (according to detailed studies performed by Mariani et al. 1979, using *Helios 1* and *Helios 2* observations). This assumption should be regarded as a first approximation (Cartwright & Moldwin 2010, for instance, found that the flux rope magnetic intensity decreases as $R^{-0.94}$, though not providing information on the magnetic field components), which, in addition, affects only the strength of the magnetic helicity content and no other inferred parameters. The interval corresponding to the simulated flux rope has been put in the middle of a longer (1024 data points) sample of white noise.

The left side of Fig. 3 shows, from top to bottom, the time profiles of the magnetic field components and intensity, referring to the synthetic flux rope as would be observed from the *Solar Orbiter*’s position on April 8, 2023. The corresponding hodogram of the two transverse magnetic field components as a function of time is displayed in the top-right panel. The bottom four right panels show, from top to bottom, the temporal evolution of the average flux-rope magnetic field strength, the portion L of the structure crossed by the spacecraft, and the probe’s heliographic latitude and heliocentric distance, along *Solar Orbiter*’s trajectory.

As expected, the intensity of the flux rope magnetic field varies along the orbit of *Solar Orbiter*, increasing at smaller heliodistances. Until about 2025, when *Solar Orbiter* is still fairly close to the ecliptic plane (its heliographic latitude remains in the range $\pm 5.5^\circ$), the flux rope would be crossed almost its entire **width** (on April 8, 2023 $L \simeq 2R_C$). By contrast, from 2025, when *Solar Orbiter* begins to lift significantly off the orbital plane, the flux rope would be

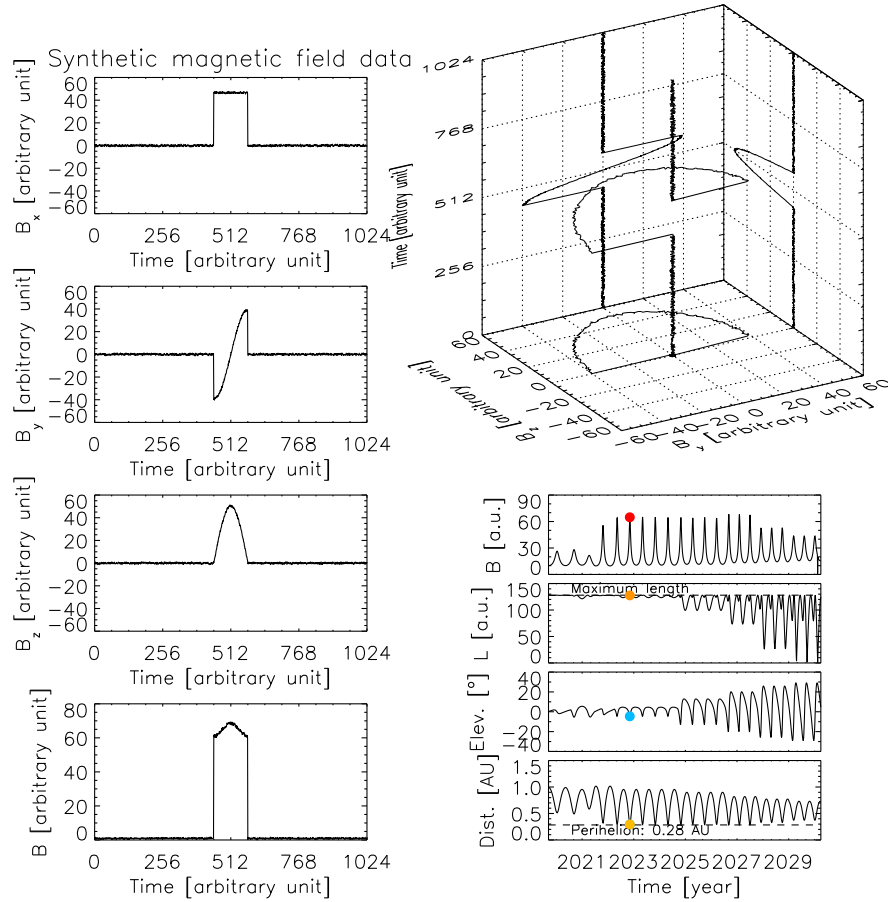


Figure 3. *Left panels:* from top to bottom, time series of the magnetic field components and magnitude, relative to the synthetic flux rope as would be observed on April 8, 2023 by *Solar Orbiter*. *Right panels:* from top to bottom, hodogram of B_y and B_z as a function of time, along with projections on the three Cartesian planes, and the average magnetic field intensity of the flux rope, portion L of the structure crossed by the probe, heliographic latitude and heliocentric distance of *Solar Orbiter*, as a function of the mission time (dots refer to April 8, 2023). [An animated version of the figure is available online.](#)

crossed only for a modest fraction, eventually, towards the end of the mission, being barely touched by the probe. The reliability of the H_m -based detection technique when only a small fraction of the flux rope is probed by the spacecraft is tested in the next section.

3. NUMERICAL TEST OF THE TECHNIQUE'S PERFORMANCE

The left side of Fig. 4 shows the magnetic helicity analysis performed on the synthetic flux rope as would be sampled from the position of *Solar Orbiter* on April 8, 2023.

Following Telloni et al. (2012) and according to Matthaeus et al. (1982), the magnetic helicity scalogram $H_m(t, \tau)$ as a function of both time t and timescale τ ($\tau = 1/\omega$, where ω is the frequency) can be expressed as

$$H_m(t, \tau) = \frac{\tau V_{\text{SW}}}{\pi} \Im[W_y^*(t, \tau) \cdot W_z(t, \tau)], \quad (2)$$

where V_{SW} is the solar wind bulk speed (assumed here not to vary and equal to 1, i.e. $V_{\text{SW}} = 1$), $W_y(t, \tau)$ and $W_z(t, \tau)$ are the Paul wavelet transforms (Torrence & Compo 1998) of the synthetic time series of the transverse magnetic components B_y and B_z (shown in Fig. 4a), and $*$ denotes the complex conjugate.

Because of its right-handed chirality (the rotation of the magnetic field vector is clockwise in the plane perpendicular to the x sampling direction), the flux rope is correctly identified as a highly positive magnetic helicity structure (Fig. 4b). From the magnetic helicity scalogram, it is possible to infer the characteristic timescale and duration of the event.

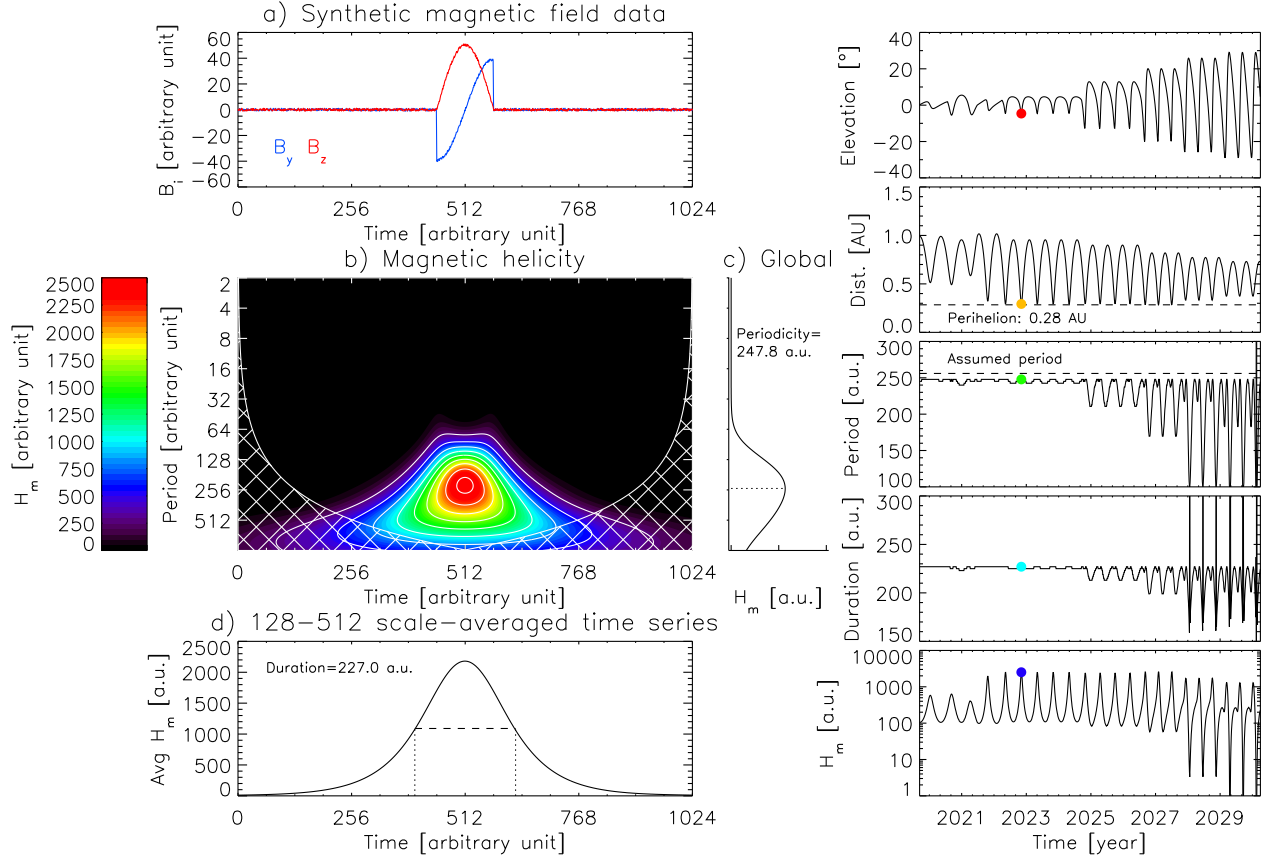


Figure 4. *Left side:* y - and z - components of the synthetic magnetic field data during the flux rope encounter as would be detected on April 8, 2023 (a); Paul wavelet magnetic helicity scalogram $H_m(t, \tau)$ (b); time-averaged magnetic helicity spectrum ($\overline{H_m}(\tau)$, c), where the characteristic timescale of the flux rope as deduced from the H_m analysis is indicated by a dotted line; scale-averaged magnetic helicity time series ($\overline{H_m}(t)$, d), where the duration of the synthetic flux rope as inferred from the FWHM of the $\overline{H_m}(t)$ profile is shown by a horizontal dashed line. *Right side:* from top to bottom, temporal evolution of *Solar Orbiter* heliocentric distance and heliographic latitude, inferred characteristic timescale and duration of the synthetic flux rope, and peak value of the flux-rope magnetic helicity, during the whole mission (dots refer to April 8, 2023). [An animated version of the figure is available online.](#)

For this purpose, it is useful to average, separately in time and timescale, $H_m(t, \tau)$ around the smallest contour inside the colored feature, thus obtaining, respectively, the time-averaged (or global) magnetic helicity spectrum $\overline{H_m}(\tau)$, and the scale-averaged magnetic helicity time series $\overline{H_m}(t)$. Specifically, $\overline{H_m}(\tau)$, shown in Fig. 4c, has been obtained by averaging $H_m(t, \tau)$ over a time interval 129 data points long centered on the flux rope event (namely at $t = 512$ data points). $\overline{H_m}(t)$, shown in Fig. 4d, is instead the result of averaging $H_m(t, \tau)$ over the timescales ranging between 128 and 512 data points. $\overline{H_m}(\tau)$ peaks at the periodicity of 247.8 data points (dotted line in Fig. 4c), in very good agreement with the assumed characteristic timescale of 256 data points (in spite of the poor frequency resolution of the Paul wavelet basis). The time duration of the synthetic flux rope, derived from the Full Width at Half Maximum (FWHM, horizontal dashed line in Fig. 4d) of the $\overline{H_m}(t)$ time series, is 227 data points, which is rather larger than the flux rope section crossed by *Solar Orbiter* on April 8, 2023 ($L = 127.6$ data points). However, it is worth noting that the determination of the flux rope duration from the H_m -based analysis strictly depends on the definition used to quantify the extent of the $\overline{H_m}(t)$ function (which in addition can have a broader or narrower shape). For instance, if the $\overline{H_m}(t)$ extent were defined as the time interval where the integral of $\overline{H_m}(t)$ is 50% of the total, then the time duration of the flux rope would be 147 data points, closer to the expected flux rope **width** L .

The right side of Fig. 4 shows, from top to bottom, the temporal evolution, during the whole mission, of the *Solar Orbiter* distance from the Sun and elevation on the ecliptic, of the characteristic timescale and duration of the flux rope inferred via the H_m analysis, and of the maximum value of the magnetic helicity content carried by the flux rope, which, as expected, is modulated by the radial dependence of the magnetic field intensity (Fig. 3).

As long as the *Solar Orbiter* remains on the orbital plane, ensuring that the flux rope will be crossed for practically its entire **width** $2R_C$, the magnetic helicity analysis would provide, for the duration and the characteristic timescale of the event, fairly constant values, in accordance with those expected (except, as already discussed, the definition used for the duration of the flux rope). However, since *Solar Orbiter* begins to have a quite inclined orbit, the values deduced from the H_m analysis begin to deviate significantly from the real values. Towards the end of the mission, when the elevation of the spacecraft exceeds 20° out of the ecliptic, meaning that the flux rope is crossed for only a small section, the analysis would provide completely unreliable results, even going so far as to be inapplicable when the flux rope is barely touched by the spacecraft. Quantitative information on the uncertainty introduced in the analysis as a function of *Solar Orbiter*'s orbital parameters and, ultimately, of the **section** of the structure crossed by the probe, is provided in the next section.

4. DISCUSSION AND CONCLUSIONS

From the results presented above, it is evident that the reliability of the diagnostic method based on the magnetic helicity analysis depends on how much of the flux rope is crossed by *Solar Orbiter*, which is a function of $R \sin \theta$, as discussed in § 2. Figure 5 shows the inferred duration and characteristic timescale of the flux rope as a function of the percentage of the structure **section** sampled by the spacecraft (top panels) and as a function of $R \sin \theta$ (bottom panels).

Regardless of which definition is adopted to estimate the dimension of the flux rope, it is clear that its duration as inferred from the magnetic helicity analysis must be proportional to the **section** of the structure effectively sampled by *Solar Orbiter*. From the top-left panel of Fig. 5, it is evident that a linear relationship exists between these two quantities if at least 50% of the structure is crossed by the probe. If less than 50% of the flux rope is sampled, it is evident that the proportionality between the inferred duration and crossed **section** is lost and therefore the H_m diagnostic technique becomes less reliable.

Similar arguments apply to the characteristic timescale of the flux rope. However, in this case the value returned by the magnetic helicity analysis should be the same as that expected (256 data points) regardless of how much of the structure has been sampled. As exhibited by the top-right panel of Fig. 5, the characteristic timescale inferred from the magnetic helicity analysis progressively deviates from the expected value as the percentage of the structure crossed decreases. The inaccuracy of the measurement is thus approximately 10% if 90% of the structure is sampled, whilst the procedure becomes totally unreliable (40% inaccuracy) if just 50% of the structure is crossed by *Solar Orbiter*.

Since the above results are expressed in terms of the percentage of the flux rope crossed by the spacecraft, they do not depend neither on its direction of propagation nor on its size, rather they are to be considered valid for any flux rope with a generic dimension transiting across the spacecraft with a generic orientation. Figure 5 not only allows the quantification of (in)accuracy of the magnetic helicity diagnostic technique, according to the orbital parameters, but, and much more important, it allows the actual values of the duration and characteristic timescale (namely, the pitch of the magnetic field winding) of the flux rope to be recovered, starting from the results obtained with the H_m analysis, once the distance from the Sun R and the inclination θ on the ecliptic of *Solar Orbiter* are known. Indeed, from the bottom panels of Fig. 5, which show, as a function of $R \sin \theta$, flux rope properties normalized to values inferred in the ecliptic plane (where 100% of the structure would be crossed and thus no inaccuracy would be introduced in the estimation), it is possible to trace back the intrinsic duration and characteristic timescale of the flux rope simply by dividing the quantities inferred at R and θ by the corresponding values reported in the bottom panels of Fig. 5.

The numerical study reported in this paper for a flux rope propagating in the orbital plane and detected by *Solar Orbiter* can be extended to a generic flux rope having any direction with respect to the position of any spacecraft. One only needs to rename θ as $\theta_{SC} - \theta_{FR}$, where θ_{SC} is the probe's heliographic latitude and θ_{FR} is the inclination of the flux rope with respect to the ecliptic. The main conclusion of this work is that, although the technique based on the computation of the MHD invariants within the flux ropes (Telloni et al. 2012) is undoubtedly powerful, special care must be taken when the inclination between the probe and the propagating structure is not negligible. It is therefore crucial to have an accurate measurement of the propagation direction of the flux rope. In this regard, observations by the Metis coronagraph (Antonucci et al. 2020) will help to quantify this parameter for structures having a solar

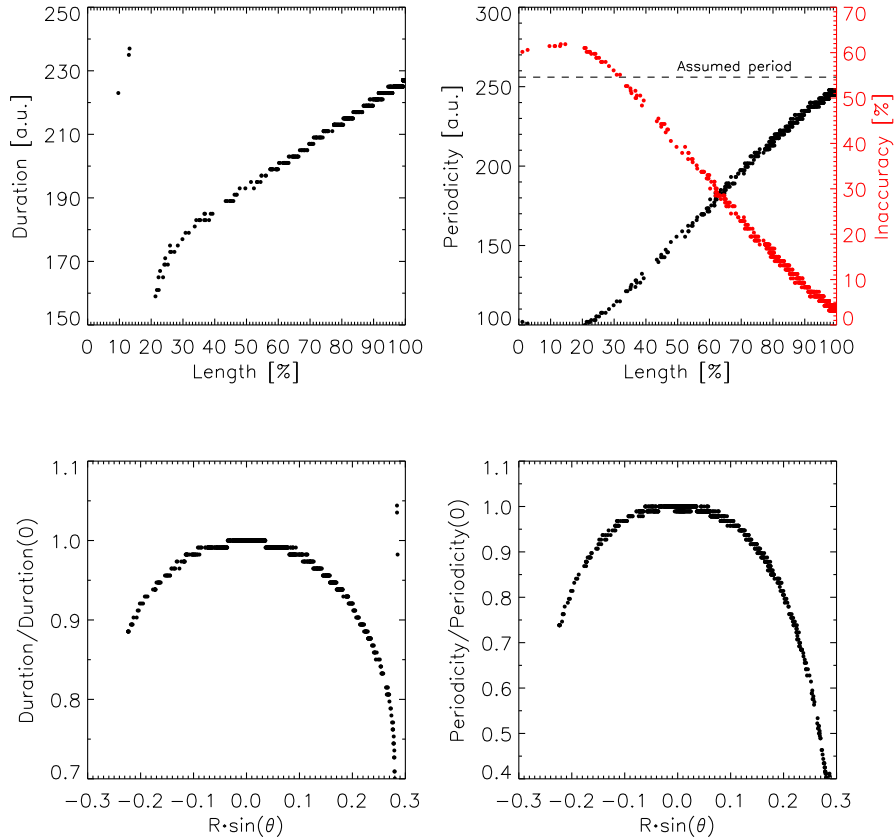


Figure 5. Flux rope duration (*left panels*) and characteristic timescale (*right panels*), as inferred from the H_m analysis, as a function of the percentage of structure size crossed by *Solar Orbiter* (*top panels*) and of $R \sin \theta$ (*bottom panels*); the measurement inaccuracy for the characteristic timescale is also illustrated (red dots).

origin. Also Grad-Shafranov (GS) reconstruction techniques (Zheng & Hu 2018; Hu et al. 2018) or velocity-modified Gold-Hoyle (GH) model approaches (Wang et al. 2015, 2016) might be exploited to measure the propagation direction of flux ropes. A numerical test based on the GS reconstruction method combined with the H_m analysis is indeed planned and is the content of an upcoming paper.

D.T. was partially supported by the Italian Space Agency (ASI) under contract I/013/12/0.

REFERENCES

- Adhikari, L., Khabarova, O., Zank, G. P., et al. 2019, *ApJ*, 873, 72
- Antonucci, E., Romoli, M., Andretta, V., et al. 2020, *A&A*, in press
- Carbone, V. & Veltri, P. 1992, *A&A*, 259, 359
- Cartwright, M. L., & Moldwin, M. B. 2010, *J. Geophys. Res.*, 115, A08102
- Chen, Y., Hu, Q., & le Roux, J. A. 2019, *ApJ*, 881, 58
- Cranmer, S. R., Kohl, J. L., Noci, G. et al. 1999, *ApJ*, 511, 481
- Feng, H. Q., Wu, D. J., & Chao, J. K. 2007, *J. Geophys. Res.*, 112, A02102
- Frisch, U., Pouquet, A., Leorat, J., & Mazure, A. 1975, *J. Fluid Mech.*, 68, 769
- Gray, T., Brown, M. R., & Dandurand, D. 2013, *PhRvL*, 110, 085002
- Goldstein, H. 1983, in *NASA Conf. Publ. 2280, Solar Wind Five*, ed. M. Neugebauer, 731
- Hu, Q., Zheng, J., Chen, Y., le Roux, J., & Zhao, L. 2018, *ApJS*, 239, 12

- Janvier, M., Démoulin, P., & Dasso, S. 2014, *J. Geophys. Res.*, 119, 7088
- Lepping, R. P., Burlaga, L. F., & Jones, J. A. 1990, *JGR*, 95, 11957
- Mariani, F., Villante, U., Bruno, R., Bavassano, B., & Ness, N. F. 1979, *SoPh*, 63, 411
- Matthaeus, W. H., Goldstein, M. L., & Smith, C. 1982, *PhRvL*, 48, 1256
- Mishin, V. V., & Tomozov, V. M. 2016, *SoPh*, 291, 3165
- Moffat, H. K. 1978, *Magnetic Field Generation in Electrically Conducting Fluids* (Cambridge: Cambridge Univ. Press)
- Parker, E. N. 1988, *ApJ*, 330, 474
- Parker, E. N. 1994, *Spontaneous Current Sheets in Magnetic Fields* (New York: Oxford Univ. Press)
- Russell, C. T., & Elphic, R. C. 1979, *Natur*, 279, 616
- Taylor, J. B. 1974, *PhRvL*, 33, 1139
- Telloni, D., Bruno, R., D'Amicis, R., et al. 2012, *ApJ*, 751, 19
- Telloni, D., Perri, S., Bruno, R., et al. 2013, *ApJ*, 776, 3
- Telloni, D., Carbone, V., Perri, S., et al. 2016, *ApJ*, 826, 205
- Telloni, D., Antonucci, E., Bemporad, A., et al. 2019, *ApJ*, 885, 120
- Ting, A. C., Montgomery, D., & Matthaeus, W. H. 1986, *PhFl*, 29, 3261
- Torrence, C., & Compo, G. P. 1998, *BAMS*, 79, 61
- Vourlidas, A. 2014, *PPCF*, 56, 064001
- Wang, Y.-M., Sheeley, N. R., Jr., Walters, J. H., et al. 1998, *ApJL*, 498, L165
- Wang, Y., Zhou, Z., Shen, C., Liu R., & Wang, S. 2015, *J. Geophys. Res.*, 14, 5
- Wang, Y., Zhuang, B., Hu, Q., et al. 2016, *J. Geophys. Res.*, 121, 9316
- Woltjer, L. 1958, *PNAM*, 44, 489
- Yu, W., Farrugia, C. J., Lugaz, N., et al. 2014, *J. Geophys. Res.*, 119, 689
- Zank, G. P., le Roux, J. A., Webb, G. M., Dosch, A., & Khabarova, O. 2014, *ApJ*, 797, 28
- Zank, G. P., Hunana, P., Mostafavi, P., et al. 2015, *ApJ*, 814, 137
- Zank, G. P., Adhikari, L., Hunana, P., et al. 2017, *ApJ*, 835, 147
- Zank, G. P., Adhikari, L., Hunana, P., et al. 2018, *ApJ*, 854, 32
- Zhao, L.-L., Zank, G. P., Khabarova, O., et al. 2018, *ApJL*, 864, L34
- Zhao, L.-L., Zank, G. P., Chen, Y., et al. 2019, *ApJ*, 872, 4
- Zhao, L.-L., Zank, G. P., Hu, Q., et al. 2019, *ApJ*, 886, 144
- Zhao, L.-L., Zank, G. P., Adhikari, L., et al. 2020, *ApJS*, 246, 26
- Zheng, J., & Hu, Q. 2018, *ApJL*, 852, L23